ACS OMEGA

Open Access

This article is licensed under CC-BY-NC-ND 4.0

http://pubs.acs.org/journal/acsodf

Article

Molecular Dynamics Computational Study of Sustainable Green Surfactant for Application in Chemical Enhanced Oil Recovery

Riyad Mahfud*

Cite This: *ACS Omega* 2024, 9, 27177−27191

Read Online

ACCESS | Metrics & More | Article Recommendations | Supporting Information

ABSTRACT: Green surfactant (GS) flooding, an environmentally friendly chemical Enhanced Oil Recovery (cEOR) method, is explored in this molecular dynamics (MD) simulation study. This study evaluates the ability of (*S*)-2-dodecanamido-aminobutane-dioic as a GS for cEOR, assessing its performance with hexane (C6), dodecane (C12), and eicosane (C20) as representative oils. In the case of the bulk system, a comprehensive molecular-level investigation provides structural details such as the radial distribution function, solvent-accessible surface area, GS adsorption dynamics, diffusivity, and emulsion stability of the GS, oil, and water systems. Also the impact of the three distinct oils on interfacial tension was examined in the existence of GS molecules. The findings reveal rapid GS molecule aggregation and adsorption on oil droplets, with various impacts on emulsion stability depending on the oil type. Additionally, GS enhances the aggregation of heavy C20 oil molecules in a water medium. The study demonstrates GS's role as an effective emulsifier, facilitating oil droplet recovery, with electrostatic interactions governing micelle formation and van der Waals interactions influencing oil droplet emulsification. These results align with prior experimental data, affirming GS's promising application potential in cEOR while prioritizing environmental sustainability.

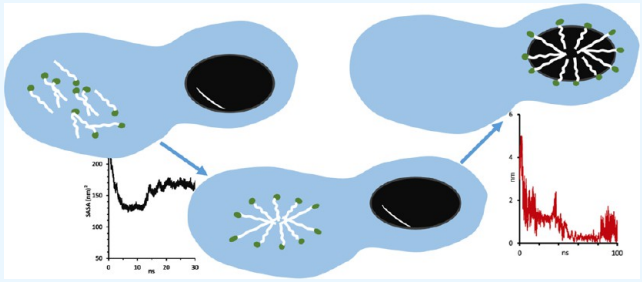

■ INTRODUCTION

The global demand for energy continues to rise, with BP's report (Dale, S., & Fattouh, B. (2022). Peak oil demand and long-run oil prices) indicating an expected increase in crude oil demand by approximately 12.9% to reach around 109 million barrels per day of oil equivalent by 2035. Meeting this demand necessitates the utilization of enhanced oil recovery (EOR) methods. The goal of EOR is to recover trapped oil, which can often represent over 50% of the original oil in place in the reservoir, even after primary and secondary recovery processes.[1,2] EOR involves the injection of chemicals, gases, or thermal energy into reservoirs to release trapped oil reserves.[3,4] Commercial surfactants are commonly employed in chemical injection enhanced oil recovery (cEOR), where they play a crucial role in reducing the interfacial tension between the injected fluids and the reservoir's oil phase.[5] The application of chemicals in EOR must consider environmental impact, including factors such as aquatic toxicity, effects on human health,[6] and low biodegradability.[7] Furthermore, the consequences of using commercial surfactants extend to adverse effects on wastewater treatment, aquatic microbial populations, fish, other aquatic organisms, and even the efficiency of plant photochemical energy conversion.[8]

In surfactant flooding, a surfactant solution is injected into the reservoir with a surfactant concentration ranging from 0.3 to 2% by weight,[9,10] which may vary based on reservoir conditions, such as temperature and salinity, to create a microemulsion solution. And in field-scale operations, surfactant consumption can annually range from 7000 to 14,000 tons (Lee, C., & Berger, P. (1998). Surfactant Injection Projects - Field Cases. Oil Chem Technologies, Inc.), making the cost of surfactants a significant factor. Additionally, addressing environmental and sustainability challenges associated with surfactant usage is crucial, and one approach to tackle these issues is through the using or adopting green surfactant (GS).

Many researchers[11−14] have utilized molecular dynamics (MD) simulations to study the behavior of commercial surfactants in cEOR. Most of these studies aim to investigate how surfactant molecules interact at the interface, as the success of the cEOR process hinges on the interactions between surface agents and crude oil.[15] To create a more environmentally sustainable future, GS has been utilized in cEOR to optimize yields while minimizing environmental impact. In laboratory experiments, GS derived from plant-based sources have demonstrated performance comparable to or better than traditional synthetic surfactants.[16−18] The fundamental principle in the cEOR process involves the dynamic interaction of

Received: February 10, 2024
Revised: May 30, 2024
Accepted: June 5, 2024
Published: June 12, 2024

ACS Publications

© 2024 The Author. Published by American Chemical Society

https://doi.org/10.1021/acsomega.4c01332
ACS Omega 2024, 9, 27177−27191

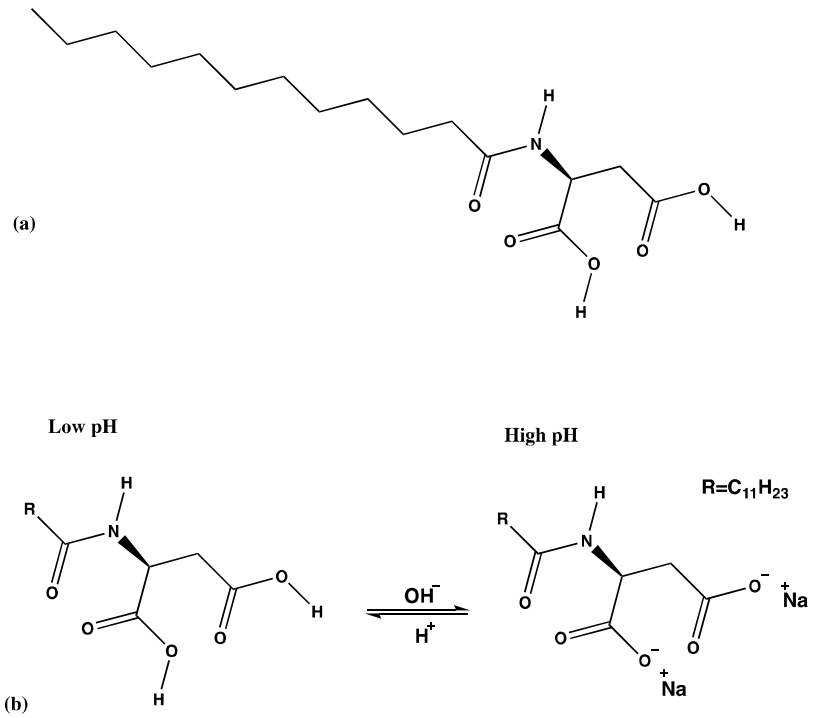

Figure 1. (a) Chemical structure of (*S*)-2-dodecanamido-aminobutanedioic, molecular weight of 315.41 amu, will be introduced as GS in this study. (b) Structure transition of GS induced by pH.

flooding agents or cEOR agents with crude oil.[15] Although there have been relatively few MD studies on the effects of GS on the emulsification of oil droplet ganglia, experimental evidence supports the idea that GS can significantly enhance oil recovery through mechanisms such as reducing interfacial tension (IFT), altering wettability, and promoting emulsification.[16,17] Despite the cost-effectiveness of GS,[19] their infrequent use in cEOR can be attributed to the limited research regarding their potential to create stable oil-in-water emulsions while meeting the essential requirements for interfacial tension and surfactant adsorption properties. An extensive review of available literature reveals a significant lack of systematic MD studies focusing on the aggregation behavior, micellar morphology, adsorption onto oil surfaces, emulsification processes, and equilibrium transport properties of these substances.

More recent work by Atilhan et al.[20] has examined the potential of using deep eutectic solvents (DES) for EOR through MD simulations. The research assesses four DES compositions based on choline chloride and various hydrogen bond donors, focusing on their impact on interfacial tension, wettability of oil droplets on calcite surfaces, and intermolecular interactions, providing insights for environmentally friendly cEOR operations with low-cost, green solvents. In a study by Wei et al.,[21] MD simulations were conducted to investigate two green surfactants—one containing dodecyl sulfate and the other containing laurate. The research focused on analyzing their self-assemblies and offered valuable insights into their potential applications for improving the solubilization of challenging substances. Suhendar et al.[22] focused on evaluating oleic acid-based surfactants combined with various lengths of polyethylene glycol for cEOR applications by using MD simulations. Their ability to reduce IFT, emulsify oil, and change rock wettability was screened.

This study selected a previously reported green surfactant (GS) characterized by a distinctive headgroup comprising two carboxylic groups, an amine group, and an oxygen atom (Figure 1a). The selected (*S*)-2-dodecanamido-aminobutanedioic is rooted in the effectiveness of polar amino acids when combined with nonpolar long-chain compounds, which is a reliable approach for creating surfactants with low toxicity and environmentally friendly properties as reported by Morán et al.[23] Amino acids inherently possess both carboxylic (−COOH) and amine (−NH) functional groups. The nature of amino acids, whether neutral, basic, or acidic, is determined by the relative strength of these functional groups. The carboxylic acid groups of the GS molecule can be protonated (−COOH) under lower pH (acidic conditions) or deprotonated ($-COO^-$) under higher pH (alkaline conditions), as illustrated in Figure 1b. Numerous amino acid-based surfactants with confirmed potential for chemical enhanced oil recovery (cEOR) have been documented in the literature.[24,25] Using MD simulations, this study investigated the GS's capacity to emulsify various types of oil droplet clusters in an aqueous medium, elucidating the processes of GS micellization and adsorption, which are essential for ensuring emulsion stability. The results obtained hold the potential to provide valuable insights and practical guidance for the effective utilization of these green surfactants in the enhancement of oil recovery processes.

■ METHODOLOGY

System Initialization. A GROMACS[26] software package has been used to carry out MD simulation processes, and the OPLS-AA[27] force field was used. All atoms were explicitly represented (including all hydrogen atoms). Various publications in the literature confirm the OPLS force field's[27−29] ability to represent complicated systems made of a variety of materials.[30−32] The OPLS_AA force field describes the bonded (bond stretching, bond angle, and dihedral angle) and nonbonded (Lennard-Jones and Coulombic) interactions in the system. The OPLS-AA force field has successfully been

https://doi.org/10.1021/acsomega.4c01332
ACS Omega 2024, 9, 27177−27191

Table 1. Details of the MD Simulation for the Bulk Systems[a]

	C6-GS-Wt	C12-GS-Wt	C20-GS-Wt
* System configuration at t=0	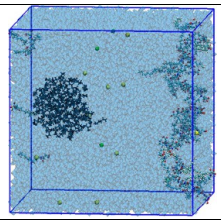	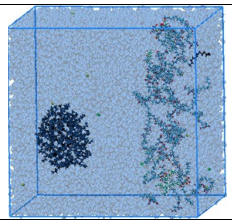	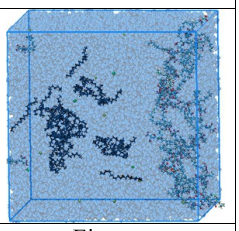
Oil model	Hexane	Dodecane	Eicosane
Oil molecules	100	50	30
GS molecules	50	50	50
Water molecules	31237	31237	31237

[a]Snapshots of the systems at time = 0: GS molecules are shown in CPK format and colored green, with red spheres representing oxygen atoms and blue spheres representing nitrogen atoms in the GS head. Oil molecules are displayed in line representation and colored black. Na and Cl ions are shown in van der Waals representation and colored in yellow and green, respectively. Water in the box is shown as a transparent surface.

Table 2. Details of the MD Simulation of the Interface[a]

	C6-GS-Wt	C12-GS-Wt	C20-GS-Wt
* System configuration at t=0	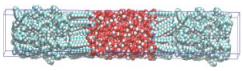	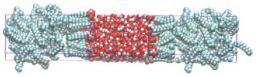	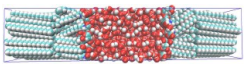
Oil model	Hexane	Dodecane	Eicosane
Oil molecules	190	78	40
GS molecules	40	40	40
Water molecules	1202	1202	1202

[a]Snapshots of the systems at time = 0: nitrogen, oxygen, and carbon belonging to GS molecules are shown in blue, red, and green by vdW drawing method in VMD, respectively; and water molecules are shown in red and white by vdW drawing method in VMD; and oil molecules are shown in green and white by vdW drawing method in VMD.

applied to different systems to predict energy of mixing, micellization process, surface tension of organic liquids, etc.[30−32] The SPC/E water model[33] was used to describe the water molecules. The MD simulations were performed by employing periodic boundary conditions (PBC) in the entire simulation box,[34] and PBC were applied in all three directions to generate a quasi-infinite solution. Simulations used the Berendsen thermostat[35] to control simulation temperature (T = 310 K), and pressure is retained with the semi-isotropic Parinello−Rahman pressure coupling (P = 1 bar).[36] With a time-step in all simulation runs of 1.0 fs, the leapfrog algorithm was utilized to solve Newton's equations of motion.[37] Nonbonded cutoff radius of 1.0 nm was adopted for nonbonded interactions to evaluate van der Waals interactions, and long-range electrostatic interactions were assessed with the particle mesh Ewald method to capture Coulomb interactions during our MD simulation.[38] These parameters have been validated and utilized for investigating the molecular behavior of crude oil.[39]

System Exploration and Simulation Details. Green surfactants are known for their tendency to adsorb at interfaces due to their dual nature. In this study, (S)-2-Dodecanamido-Aminobutanedioic was selected as a surface-active agent to investigate the emulsification behavior of various types of oil droplets. Figure 1 provides a schematic representation of the chemical structure of the green surfactant used in this study. Further information on the synthesis and preparation procedures for (S)-2-Dodecanamido-Aminobutanedioic can be found in the literature.[40] Given that oil droplets are complex mixtures containing numerous hydrocarbon compounds, representative model compounds can be employed to effectively simulate their structures. In this study, hexane, dodecane, and eicosane were selected as representative model compounds to simulate different oil droplets. The aggregative behavior of these selected compounds in aqueous media was assessed. To create the oil droplets in the three systems, oil molecules were solvated with an equivalent number of water molecules (31237 molecules), while ensuring that the total number of carbon atoms in the oil systems remained constant (600 atoms). Any net charge was neutralized by adding an appropriate number of Na^+ (10 sodium ions) and Cl^- ions (4 chlorine ions). As an initial step, energy minimization was performed by using the steepest descent algorithm until the maximum force in the system reached values less than 0.001 N/mol (1000 kJ/mol/nm). MD simulations were conducted in two ensembles: the NVT ensemble (constant number of particles N, volume V, and temperature T) and the NPT ensemble (constant N, pressure P, and temperature T). Each ensemble was simulated for 2000 ps to equilibrate the system at a temperature of T = 310 K and a pressure of P = 1 bar with coupling time constants of 0.1 and 1.0 ps, respectively. Following equilibration, a 4 ns MD production run was carried out at T = 310 K and P = 1 bar. The resulting trajectories from this production run were used as the initial coordinates for the oil/water/GS systems. Three distinct systems were designed to assess the emulsifying capabilities of GS. In these simulation boxes, GS molecules were initially distributed at approximately equidistant positions from the oil droplets. Notably, the final structure of the oil molecules served as the initial coordinate for the oil/water system. Further details

https://doi.org/10.1021/acsomega.4c01332
ACS Omega 2024, 9, 27177−27191

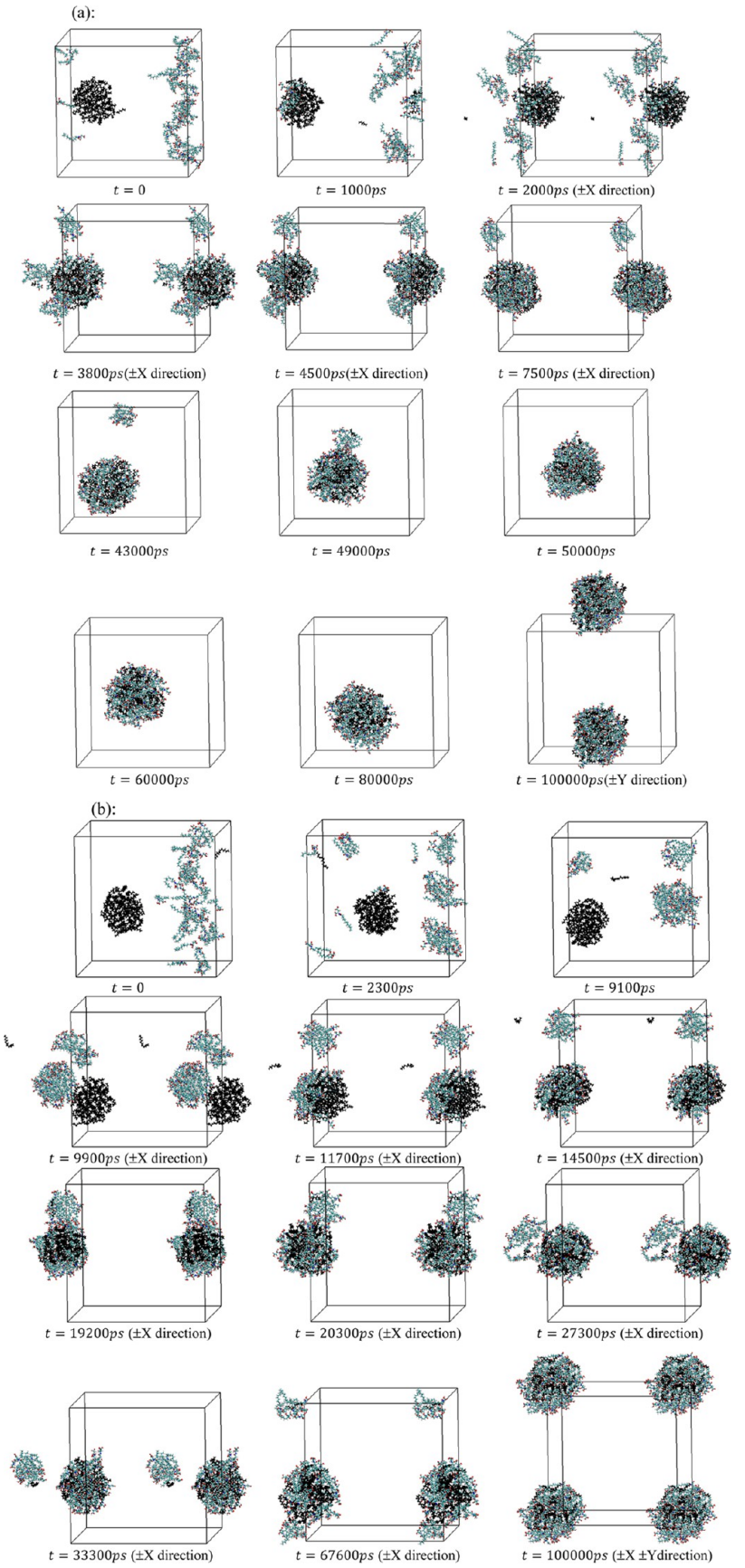

Figure 2. continued

https://doi.org/10.1021/acsomega.4c01332
ACS Omega 2024, 9, 27177−27191

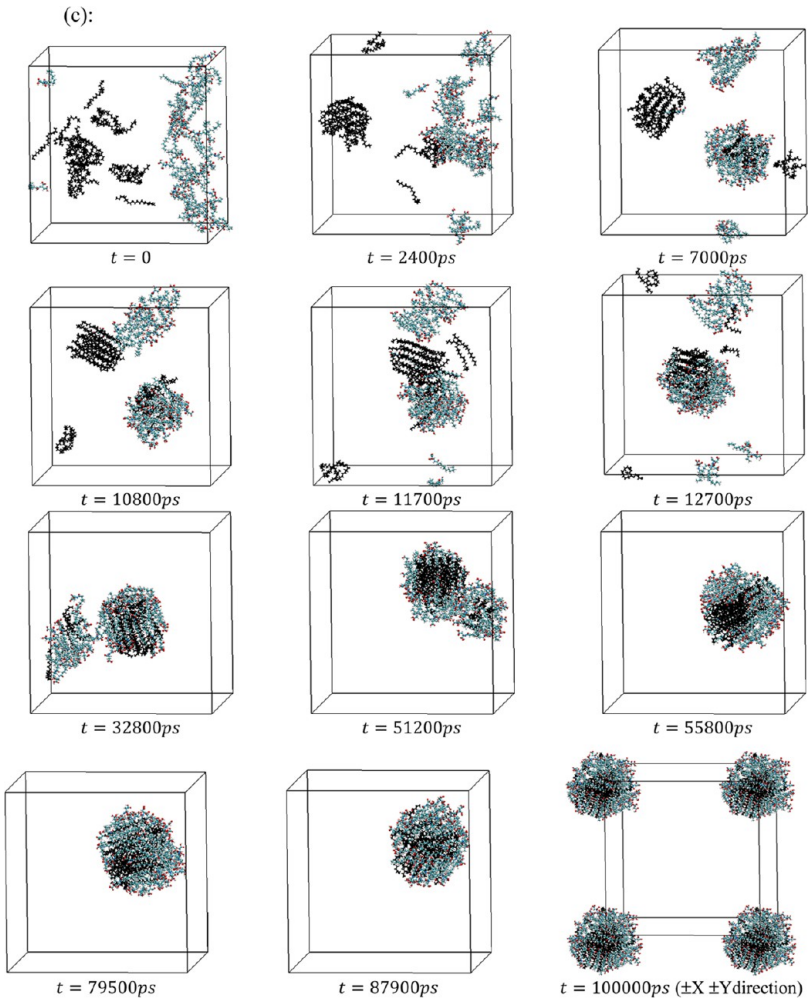

Figure 2. Snapshots depicting the spontaneous aggregation of GS molecules (at a concentration of 8.3 M) into spherical micelles and the subsequent dissociation of GS molecules, forming micelles around the oil droplets. GS molecules are represented in CPK format and colored green, with red spheres representing oxygen atoms and blue spheres representing nitrogen atoms in the GS head. Oil molecules are displayed in line representation and colored black. Ions and water molecules have been omitted for clarity. (a) Configuration diagrams at different simulation times in the C6-GS-Wt system. (b) Configuration diagrams at different simulation times in the C12-GS-Wt system. (c) Configuration diagrams at different simulation times in the C20-GS-Wt system. Periodic images in VMD were selected to include complete images within the unit cell, encompassing both ±X and/or ±Y directions.

about the simulation boxes can be found in Table 1. The dimensions of the simulation box were uniform for all systems, measuring $10 \times 10 \times 10$ nm^3. Each simulation run had a total duration of 100 ns. Subsequently, the MD trajectory was visualized and analyzed by using Visual Molecular Dynamics (VMD, Version 1.9.4). Additional MD simulations were conducted for the deprotonated ($-COO^-$) GS molecules under similar conditions as before to investigate the effect of pH on the hydration of the amine group. In these simulations, 100 Na^+ ions were added to replace the 100 H^+ protons in the carboxylic groups and an appropriate number of Cl^- ions were added to neutralize the net charge.

The interfacial tensions were determined using isobaric−isothermal ensemble and applying periodic boundary condition. The simulation cells were created using orthorhombic boxes with side dimensions $L_y = L_x = 3$ nm, and L_z approximately five times longer. In the initial configuration, a water film was sandwiched between two layers of oil, each containing dispersed green surfactants at the interfaces. All systems utilized a similar considerable number of water molecules, and the quantity of GS molecules was maintained at a consistent level. In Table 2, C6 oil molecules were used in high quantities to ensure that all of the surfactant atoms along the chain length interacted with the oil molecules, whereas C12 and C20 oil molecules are long enough to establish significant interactions with the surfactant chains. This approach allows observation of the effects of changes in the oil composition within the system. Additionally, sodium ions were introduced into each system to balance the overall charge, with detailed information available in Table 2. The molecular packing program Packmol[41] was used to build the GS monolayers with a fully packed monolayer at the water−oil interface. All systems were initially placed in a $3 \times 3 \times 14$ nm box; the initial structure is shown in Table 2. 1 ns simulation with NVT ensemble is used to achieve the desired temperature, 315 K, followed by a 1 ns simulation with NPT ensemble under 1 atm. Finally, a 10 ns simulation was performed, and the data in the last 5 ns were collected for analysis. All of the simulations were conducted using the molecular dynamics parameters as previously described.

https://doi.org/10.1021/acsomega.4c01332
ACS Omega 2024, 9, 27177−27191

RESULTS AND DISCUSSION

The bulk systems under study each consist of an equal number of carbon atoms, specifically 600 atoms; this consistency ensures that any observed differences in the system behavior can be attributed primarily to variations in the oil molecules structures rather than differences in oil concentration. Oils with relatively low molecular mass are represented by a chain length of 6 carbon atoms, oils with a medium molecular mass are represented by a chain length of 12 carbon atoms, and oils with a relatively large molecular mass are represented by a chain length of 20 carbon atoms. In all three systems, 50 molecules of green surfactants (GS) were introduced, as detailed in Table 1. The total simulation duration of 100 ns via free molecular dynamics allows for an atomic-level description of GS micellization and micelle formation around the oil droplets within these three systems. Snapshots of the simulation systems are illustrated in Figure 2. In each system, there were 50 GS molecules, corresponding to a concentration of approximately 8.3 M. It is worth noting that the critical micelle concentration value of GS is approximately 0.82 M.[40] The absence of water molecules in Figure 2 aims to provide a clearer visualization of GS micellization and the formation of GS micelles around the oil droplets. Initially, GS molecules were randomly inserted on one side of the simulation box, while the oil droplet was placed on the opposite side, resulting in the isolation of most GS molecules. Over the course of simulations, the surfactants quickly self-associated into small cluster-like micelles that adsorb to the oil droplet surface. At t = 10 ns, spontaneous aggregation of GS molecules into small micelle-like clusters was observed, which formed at various positions in the C12-GS-Wt and C20-GS-Wt systems. Figure S1 presents a series of snapshots illustrating the spontaneous aggregation process at various time points (t = 10, 20, 30, 40, 50, 60, 70, 80, 90, and 100 ns). In contrast, in the C6-GS-Wt system, GS molecules had already emulsified with the oil droplet by 10 ns, as further visual investigations revealed in Figure 2. Over time, GS molecules in the small micelle-like clusters rapidly became absorbed onto the surface of the oil droplets. By the last 50 ns of the simulation, there were no free GS molecules in the aqueous media, indicating that the systems had reached equilibrium and stability. This behavior, where the polar heads of GS molecules enter the water phase while their tail chains remain stretched in the oil phase, as shown in the snapshots, can be attributed to the dependence of micelle formation on molecular interactions,[42] particularly short-range forces.[43]

The root-mean-square displacement (RMSD) quantifies the deviation in atomic coordinates from their initial positions. It tracks the displacement of individual components relative to their initial states and provides insights into the motion of substances within the system.[44] RMSD values were used to assess the thermodynamic equilibrium of the system and were calculated using the following formula:

$$\mathrm{RMSD} = \sqrt{\frac{1}{N}\sum_{i=1}^{N}\langle |r_i(t) - r_i(0)|\rangle^2} \quad (1)$$

where N is the total number of atoms in the system, $r_i(t)$ is the position coordinate of the i-th atom at time t, and $r_i(0)$ is the initial position coordinate of the i-th atom.

The RMSD values for GS molecules in water/oil systems are shown in Figure 3, revealing distinct trends over the course of the simulation. Notably, it becomes evident that the time required to achieve stable GS structural formations is approximately 50 ns for all three systems. Beyond this point, the RMSD values reach a constant value and remain stable for the rest of the 50 ns of the simulation. During the initial 5 ns, the RMSD values of GS molecules in the three systems exhibited rapid fluctuations, transitioning between high and low values. These fluctuations reflect various molecular interactions as the systems undergo changes in their conformation and dynamic behavior. The RMSD initially rises as the GS molecules gather into micelle-like clusters at specific time points, such as at 0.3, 0.5, and 0.9 ns, as depicted in Figure S2. The rearranging of GS molecules as they attempt to obtain a stable conformation from these micelle-like clusters is likely to be the cause of the increase in RMSD. The RMSD drops to lower values for other time intervals, such as those between 8 and 10 ns, indicating minimal structural change. As seen in Figure 2, GS molecules are absorbed by the oil droplet when the micelle-like clusters approach it. This absorption results in the hydrophobic tails facing inward toward the core of the oil droplet and the hydrophilic heads facing outward toward the aqueous medium. Consequently, the RMSD values of GS molecules exhibit fluctuations as they undergo structural transitions, stabilizing at around 50 ns when the entire system reaches equilibrium in the oil droplet configuration. After 50 ns, the RMSD values for the three systems were calculated, yielding averages of approximately 4.6, 3.8, and 4.1 nm for C6-GS-Wt, C12-GS-Wt, and C20-GS-Wt, respectively. From the RMSD analysis of GS in the three systems, it is evident that GS molecules played a crucial role in promoting the spontaneous formation of stable micelles during the emulsification process. Specifically, the lower RMSD values observed for C12-GS-Wt compared to those of C6-GS-Wt and C20-GS-Wt indicate a higher degree of structural stability within the C12-GS-Wt system. This enhanced stability contributed to the improved emulsification of various oil types, thereby promoting the overall stability of the resulting emulsions and microemulsions.

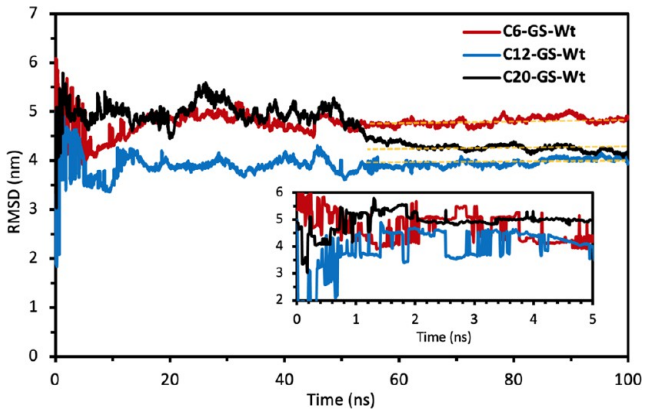

Figure 3. Time evolution of root-mean-square deviation (RMSD) of GS molecules in an oil/water system with different oil types.

The solvent accessibility surface area (SASA) values of the three systems were analyzed to assess changes in the surface of the GS molecules. SASA represents the surface area of the molecule that is accessible to solvent molecules.[44] The Shrake and Rupley algorithm[45] was employed to determine the SASA of the GS molecules. This algorithm discretizes the surface of the GS molecule into grid points and utilizes a probe sphere to traverse the surface. Grid points are then checked to determine if they are accessible or inaccessible to solvent molecules. SASA represents the surface area accessible to water atoms and is

https://doi.org/10.1021/acsomega.4c01332
ACS Omega 2024, 9, 27177−27191

calculated based on the distance from grid points to all atoms of the GS molecule. If the distance is greater than the sum of the probe sphere radius and the GS molecule atom radius, it is considered to be accessible. Finally, the accessible surface areas are summed to obtain total SASA.

The solvent accessibility surface area (SASA) analysis of C6-GS-Wt, C12-GS-Wt, and C20-GS-Wt systems throughout the simulation revealed a consistent trend, as shown in Figure 4.

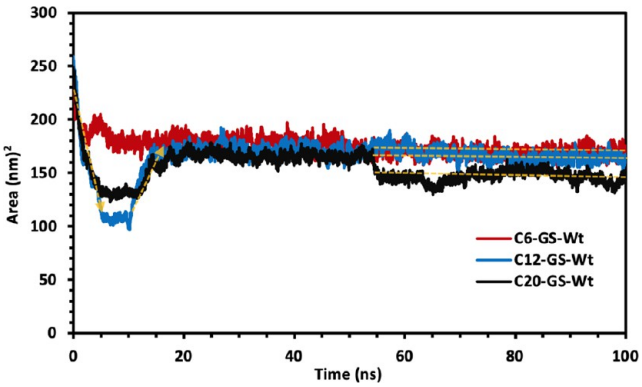

Figure 4. Variations of the solvent accessibility surface area (SASA) in oil-GS-water systems as a function of simulation time.

While the stabilization of SASA values after 20 ns suggests equilibrium within the systems, it does not directly correlate with improved emulsification performance. Notably, analysis of SASA fluctuations, particularly during the initial emulsification stages (before 20 ns), offers more informative insights. Initially, all systems exhibited a decrease in the SASA as GS molecules aggregated into small clusters and began emulsifying the oil droplet, minimizing contact with water molecules. The minimum SASA observed at 2.2 ns for the C6-GS-Wt system indicates cluster aggregation (as illustrated in Figure 2), followed by a peak at 5.2 ns, suggesting absorption of GS molecules onto the oil droplet surface. These processes were accelerated in the C6-GS-Wt system due to its higher dynamic motion compared to those of other molecules. The subsequent increase in SASA values for all systems postemulsification indicates an expanded surface area for interactions with water molecules. Notably, lower SASA values observed for C20-GS-Wt at specific time points (55 and 95 ns) can be attributed to hydrophobic chain rearrangements, as will be further discussed. Ultimately, SASA values stabilized around 20 ns, reaching equilibrium values of 167, 159, and 148 nm^2 for C6-GS-Wt, C12-GS-Wt, and C20-GS-Wt, respectively, suggesting that GS molecule conformational structures reached equilibrium during the simulation. This SASA analysis provides critical insights into the dynamic behavior of GS molecules during emulsification, emphasizing the importance of early-stage fluctuations in understanding system behavior and potential correlations with emulsification performance.

To further investigate the use of GS molecules in emulsifying oil droplets in water, the distances between the center of mass (COM) of GS molecules and the center of mass (COM) of oil molecules were calculated, as shown in Figure 5. Determining these distances in the surfactant-oil−water system is crucial for a detailed understanding of the oil emulsification process. Both hydrogen bonds and hydrophobic interactions play key roles in reducing the distance between GS molecules and oil molecules, facilitating the oil emulsification process in water.[46] For all three

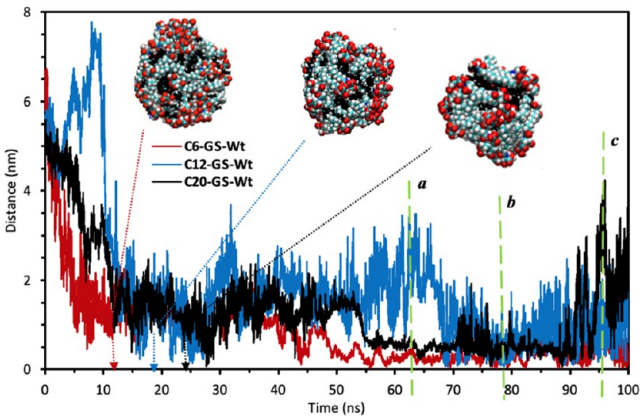

Figure 5. Distance as a function of time between the centroid of the GS molecules and the centroid of the oil molecules. The various colored arrows indicate the moments when the GS molecules emulsified the oil droplet in water. These critical points are further illustrated by three snapshots, where red spheres denote oxygen atoms, blue spheres represent nitrogen atoms in the GS head, and oil molecules are depicted in black. The system configurations corresponding to the green dashed lines (a−c) can be observed in Figure 6.

systems, as GS molecules adsorb onto the oil droplets, the distance between the GS micelles and the oil droplet gradually decreases until it reaches a minimum value, indicating that the systems approaches equilibrium. In the C12-GS-Wt system, there is a notable increase in the distance between GS and oil molecules around 8 ns due to the self-assembly and disassembly of the GS clusters, as illustrated in Figure S2. However, the high distance observed in the same system at 63 ns, represented by the green dashed line in Figure 5, can be attributed to a decrease in interactions among the oil molecules as they coalesce during the oil droplet emulsification process. This reduction in interactions can have an impact on emulsion stability.[47] Similar behavior was also observed at 95 ns, represented by dashed line c, for all three systems. Figure 6 provides images at 63, 78, and 95 ns for all systems. The oil-only images illustrate how oil molecules interact with each other on spherical droplets, minimizing their contact with water molecules. In contrast, the Oil+GS images demonstrate how GS molecules are absorbed around the oil droplets, stabilizing the emulsified oil droplets in water. The high distance values observed at 95 ns are attributed to the rearrangement of the hydrophobic chain of the GS molecules, which affect the interaction between oil molecules, as noticed by the oil-only images in Figure 6, where the oil molecules are not strongly attracted to each other as a result of being penetrated by the GS hydrophobic chain.

One of the key analyses in studying surfactant solvation, micelle formation, and oil emulsification involves the distribution of molecules, such as GS molecules, around the emulsified oil droplets. This can be accomplished by calculating the radial distribution function (RDF), denoted as $g(r)$. The RDF is defined as the probability of locating particle j within the range ($r + dr$) of particle i. The following formula was used:[48]

$$g_{ij}(r) = \langle \rho_j(r) \rangle / \langle \rho_j \rangle_{\text{local}} \tag{2}$$

where $\langle \rho_j(r) \rangle$ represents the local particle density of type j at a distance r from particle i, while $\langle \rho_j \rangle_{\text{local}}$ signifies the average particle density of type j across all spheres centered on particle i with a radius of r_{max}.

https://doi.org/10.1021/acsomega.4c01332
ACS Omega 2024, 9, 27177−27191

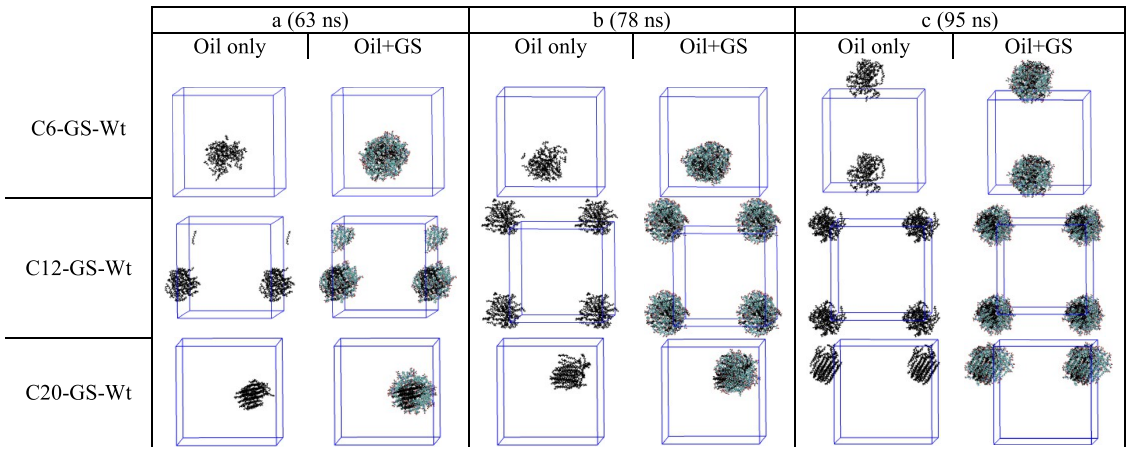

Figure 6. Snapshots depicting the configurations of the oil-GS-water systems at 63, 78, and 95 ns. GS molecules are presented in CPK representation and colored green, with red spheres representing oxygen atoms and blue spheres representing nitrogen atoms in the GS head. Oil molecules are displayed in line representation and colored black. The GS molecules are shown as being absorbed around the oil droplets. To enhance clarity, ions and water molecules have been omitted. The periodic images in the VMD are selected to include complete images within the unit cell. Specifically, some selected periodic images to draw encompass both the ±X and ±Y directions.

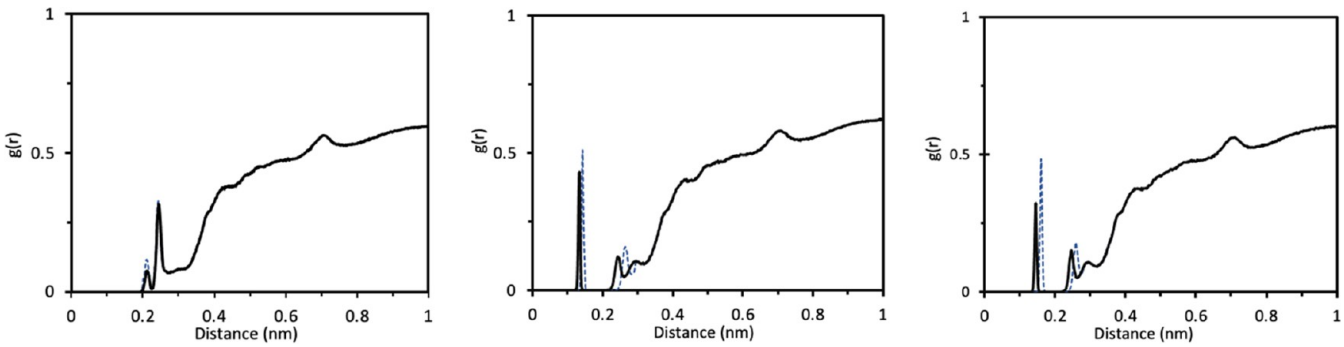

Figure 7. Radial distribution function (RDFs) between N atoms of green surfactant and oxygen atoms of water at 310 K and 1 bar for the C6-GS-Wt system (left), C12-GS-Wt system (middle), and C20-GS-Wt system (right). Comparison between protonated (solid lines) and deprotonated (dashed lines) GS molecules.

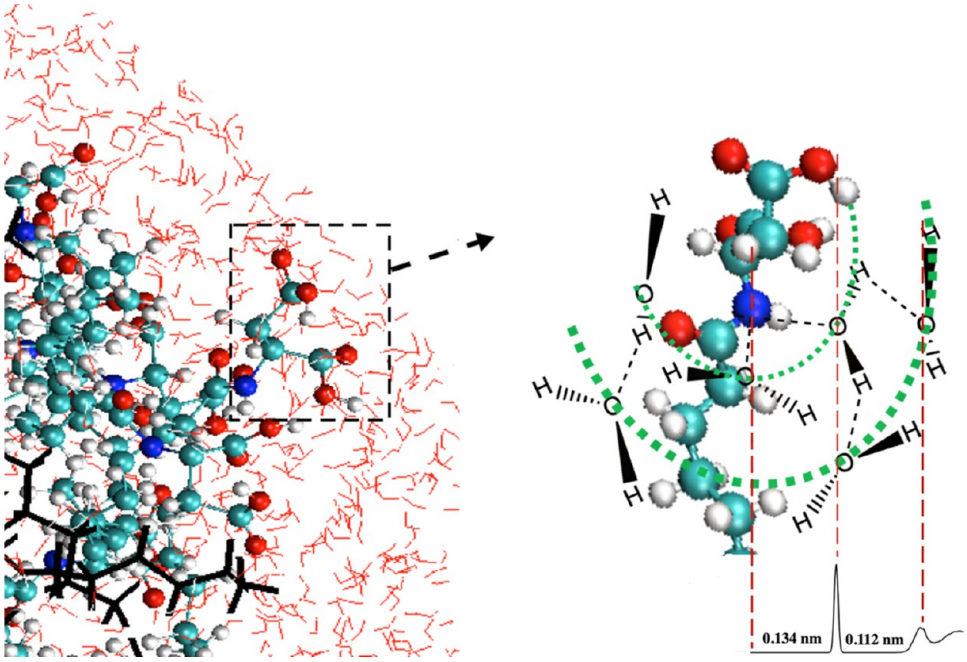

Figure 8. Radial distribution function between polar nitrogen of GS molecule and oxygen in water molecules and scheme of hydrogen bond structure in hydrogen shells.

https://doi.org/10.1021/acsomega.4c01332
ACS Omega 2024, 9, 27177−27191

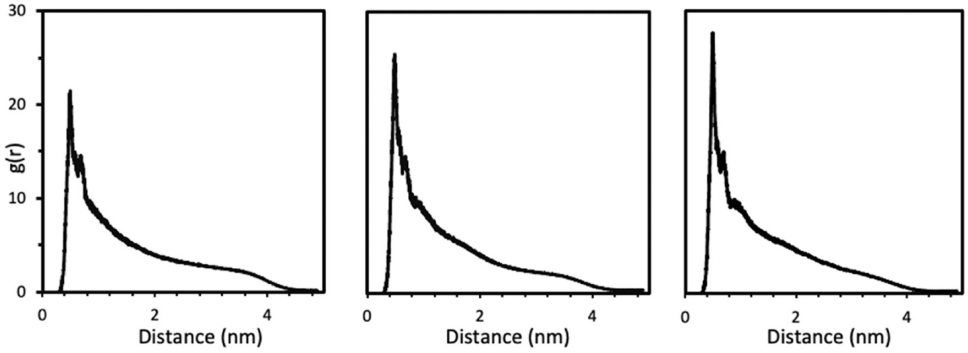

Figure 9. Radial distribution function between the N atoms of the GS at 310 K and 1 bar for the C6-GS-Wt system (left), C12-GS-Wt system (middle), and C20-GS-Wt system (right).

The radial distribution function (RDF) between the polar nitrogen atom in GS head groups and oxygen atom in water was calculated to investigate the solvation of GS molecules. Figure 7 illustrates the RDF of the water oxygen atom (Wt(O^-)) relative to the nitrogen atom in GS (N^+) for both protonated and deprotonated GS molecules. For the protonated GS molecules, the heights of the first peaks for the C6-GS-Wt and C20-GS-Wt systems were nearly identical. However, the peak positions exhibited variations among the C6-GS-Wt, C12-GS-Wt, and C20-GS-Wt systems, with peak values at 0.242, 0.134, and 0.146 nm, respectively. These peaks represent the position of the initial solvation shell surrounding the surfactant head groups, indicating strong hydration of the head groups of GS molecules by water molecules. A smaller second peak at positions corresponding to the second solvation shell was observed at 0.734 nm (C6-GS-Wt), 0.286 nm (C12-GS-Wt), and 0.288 nm (C20-GS-Wt). Additionally, only the C12-GS-Wt and C20-GS-Wt systems exhibit a small third peak at about 0.73 nm, suggesting a different solvation arrangement around the GS head groups compared to the C6-GS-Wt system. As seen in Figure 7, the C12-GS-Wt system's first peak is a bit higher than those of the other two systems. Regarding the deprotonated GS molecules, Figure 7 shows a slight increase in the intensity of the first hydration shell with a shift away from the amine group. This observation may result from intramolecular interactions at high pH between the amine group and the deprotonated carboxylic group, altering the hydration behavior compared to the protonated GS molecules. Furthermore, Figure S3 suggests that the interactions between the surfactant head groups and the surrounding water molecules are enhanced via hydrophobic interactions. This effect is likely influenced by the chain length of the GS tail, which appears to be more compatible with the chain length of the oil molecules in the C12-GS-Wt system compared to the other two systems. Therefore, it can be agreed that the presence of oil significantly contributes to this particular observed consequence.[49] In addition, Figure 8 illustrates the scheme of hydrogen bond structure within the hydration shells, as expected from the GS(N^+)-Wt(O^-) RDF of the C12-GS-Wt system. The presence of nitrogen (N) in the heads of the GS molecules enhances the number of hydrogen bonds established between the GS molecules and nearby water molecules; see Figure S4. This intermolecular interaction enhances the stability of emulsified oil molecules in water. Consequently, it can be concluded that emulsions stabilized by GS surfactants effectively enhance oil recovery.

The results of the RDF analysis between the N atoms of the head groups of GS molecules are presented in Figure 9. Notably, at short distances (ca. 0−0.48 nm), $g(r)$ remains at zero due to the strong repulsion among GS head groups.[50] In the RDF plot for all three systems, there is a prominent peak at a distance of ∼0.48 nm. This peak indicates the stronger interaction of GS molecules with emulsified oil molecules in water. Analyzing the radial distribution function (RDF) plot in Figure 9 for the oil droplet emulsification in water, we observe that the highest concentration of GS molecules falls within the range of approximately 0.44 to 1.1 nm. This concentration distribution suggests that GS molecules are concentrated around the oil droplets, confirming the aggregation behavior of GS molecules and the solubilization of oil droplets within the GS micelle.

To further characterize the translational motions of GS molecules, the mean-square displacement (MSD) was analyzed. The MSD is defined as[51,52]

$$\mathrm{MSD} = \frac{1}{N}\langle \sum_i |\vec{r}_i(t) - \vec{r}_i(0)|^2 \rangle \tag{3}$$

The MSD and self-diffusion coefficient (D_i) serve as metrics for assessing the mobility of the molecule.[53] The MSD of GS molecules was calculated by considering the GS molecule atom positions in eq 3, and the results are presented in Figure 10.

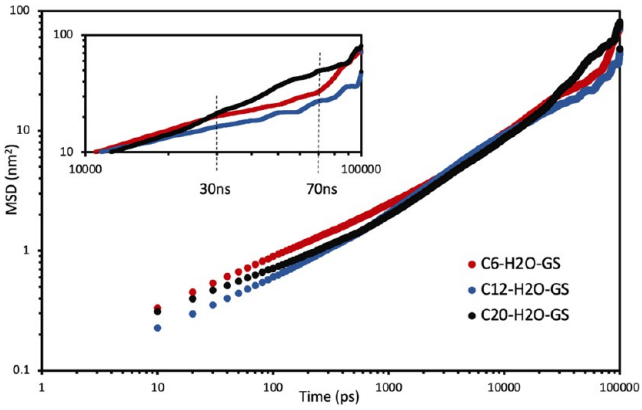

Figure 10. Mean-square displacement (MSD) of the GS molecules in the three systems shows similar diffusive behavior at the aggregation period until they reach the period of the oil droplet emulsification, which started when the GS molecules adsorbed to the oil droplet surface. This feature is related to the different intermolecular interaction of the emulsified oil molecules in water that we see in Figure 7 and which confirms the solubilization of oil droplets in the GS micelle.

https://doi.org/10.1021/acsomega.4c01332
ACS Omega 2024, 9, 27177−27191

All of the systems exhibit three distinct dynamic regimes, as evident from the MSD curves. In the first regime, there is a slow, linear increase in the MSD with simulation time, up to ∼30 ns. During this initial period (below 30 ns), the diffusion process displays subdiffusive behavior, as indicated by the shallow slope of the MDS curves. This behavior reflects the migration ability of GS molecules in aqueous media containing different types of oil. However, the second regime in the C6-GS-Wt system becomes more visible as time progresses, with a prominent shoulder extending for ∼70 ns. As seen in Figure 10, the slope of the MSD curve during the second regime is smaller than that of the first regime. This reduction in slope can be attributed to the slowed movement of GS molecules, which occurs as they become adsorbed onto the surface of the oil droplet. As is evident in Figure 2, our visual inspections of MD trajectories reveal the mechanism of GS molecule migration, aggregation, and eventual adsorption onto the oil droplet surface. Additionally, the third regime of the C6-GS-Wt system becomes apparent when the slope of the MSD plots undergoes a sharp change and increases after complete adsorption of all GS molecules onto oil droplet surface. This clearly demonstrates the system's ability to create stable oil/water emulsions, which is desirable in cEOR for effectively recovering trapped oil through chemical flooding.[54] Furthermore, in the MSD plots of the C12-GS-Wt and C20-GS-Wt systems, small shoulders and subsequent plateaus appear, indicating the presence of second regimes. Upon closer examination of both Figures 10 and 2, it becomes evident that compared to freely moving GS molecules, the mobility of emulsified oil droplets is limited, suggesting that the adsorption of GS molecules onto C12 and C20 oil droplets is slower than that on the C6 type. The short shoulders following each plateau are related to the gradual assembly and disassembly of GS molecules from the oil droplet surface, leading to the rearrangement of oil molecules. Subsequently, the third regime in the C12-GS-Wt and C20-GS-Wt systems becomes apparent as the slope of the MSD plots sharply increases once all of the GS molecules have completed the adsorption process. The diffusivity, or self-diffusion coefficient (D_i), of the different emulsified oil droplets is calculated by determining the slopes of the MDS plots during the last 5 ns of MD data. The calculated diffusivities are as follows: 0.001×10^{-5} cm^2/s for C6, 0.00095×10^{-5} cm^2/s for C12, and $0.00055 \times {}^{-5}$ cm^2/s for C20 oil types. These values are in good agreement with experimental data for similar microemulsions made from CTAB (cetyltrimethylammonium bromide)-Octane-Water, where D_i was measured as 0.00085×10^{-5} cm^2/s at 300 K.[55] In practical terms, this means that C20 emulsion droplets have a slower rate of dispersion in aqueous media compared with C12 and C6 emulsion droplets. This property can be desirable in creating emulsions that remain in the reservoir for an extended period, enhancing sweep efficiency during the cEOR process.

Since the three systems formed emulsified oil droplets and microemulsions, these emulsions facilitated the easy transport of oil droplets through porous media, consequently enhancing oil recovery. The interfacial tensions (IFT) associated with the oil/water interface play a significant role in recovery of trapped oil, prior research demonstrates that a decrease in interfacial tension can lead to an increase in oil recovery. A significant finding in the simulation result was that surfactant causes various interfacial pressure at oil/water interface.[56,57] The following formula was used for calculating the IFT of the three systems[58−60]

$$\gamma(t) = \frac{1}{2}\int_0^{L_z}\left\{P_{zz}(z,t) - \frac{P_{xx}(z,t) + P_{yy}(z,t)}{2}\right\}\mathrm{d}z \quad (4)$$

$$= \frac{L_z}{2}\left\{P_{zz}(t) - \frac{P_{xx}(t) + P_{yy}(t)}{2}\right\} \quad (5)$$

where L_z represents the box height on the Z-axis, and $P_{xx}(t)$, $P_{yy}(t)$, and $P_{zz}(t)$ denote pressure values in the X, Y, and Z directions during the simulation time. The snapshots of the arrangement of GS surfactant monolayers in the oil/GS/water/GS/oil systems are displayed in Table 2. Since the two surfactant monolayers can function independently without affecting each other, the dual-interface model effectively simulates the aggregation behavior at the two-layer oil/water interface. The Z-axis average density profiles of water, GS, and oil are shown in Figure 11, and they can be used to investigate detailed molecular distributions. Every system consists of two phases with two well-defined interfaces. The density of water bulk in three systems is 996.2−997.5 kg/m^3, the density of hexane bulk is 660.4−659.1 kg/m^3, the density of dodecane bulk is 751.2−755.3 kg/m^3, and the density of eicosane bulk is 788.2−791.4 kg/m^3, which are close to the actual density at 315 K and could initially assess the validity of the simulation system.[61] The highest peaks represent the density of GS molecules at the oil−water interface. These peaks reflect the associated hydrophobic interactions between GS molecules and oil molecules as well as the hydrophilic interactions between GS molecules and water molecules, as clarified in more detail in the analysis that follows.

The IFT values in Figure 12 show a clear trend: As the oil type becomes heavier, the IFT increases. The IFT of the C12-GS-Wt system slightly increases by 0.2 mN/m (8%) compared to the system C6-GS-Wt with lighter oil. Additionally, the IFT of the C20-GS-Wt system significantly increases by 4.7 mN/m (188%) compared to the system C6-GS-Wt system with lighter oil, despite having a similar number of GS molecules. Notably, these IFT values closely align with experimental data obtained from a system that includes the same surfactant, water, and crude oil, where the IFT was measured at 9.8 mN/m. In the experimental system, the crude oil was a mixture comprising varying percentages of saturates, aromatics, resins, and asphaltenes.[40] Thus, the variation in the hydrophobic phase's chemical structure exhibits a well-established trend in affecting interfacial tension. This observation suggests that interfacial tension is primarily governed by the hydrophobic interactions among the oil molecules,[62] rather than being primarily influenced by the strength of hydrogen bonds involving the hydrophilic segments of GS molecules and the aqueous medium. However, as illustrated in Figure 2, when considering the effects of the oil phase on surfactant adsorption, and surfactant assembly, the findings of this study align with the observations made in the existing literature.[62]

During the MD simulation, the interaction energies among GS (surfactant), oil, and water molecules are calculated to conduct a quantitative analysis of the micellization, adsorption, and emulsification processes. The surfactant micellization, as well as the adsorption of surfactant molecules and micelle molecules onto the oil droplet surface, are mainly caused by nonbonded interactions, particularly electrostatic interactions (Coulombic forces) and van der Waals interactions (Lennard-Jones forces). The interaction energies of N particles are given by

https://doi.org/10.1021/acsomega.4c01332
ACS Omega 2024, 9, 27177−27191

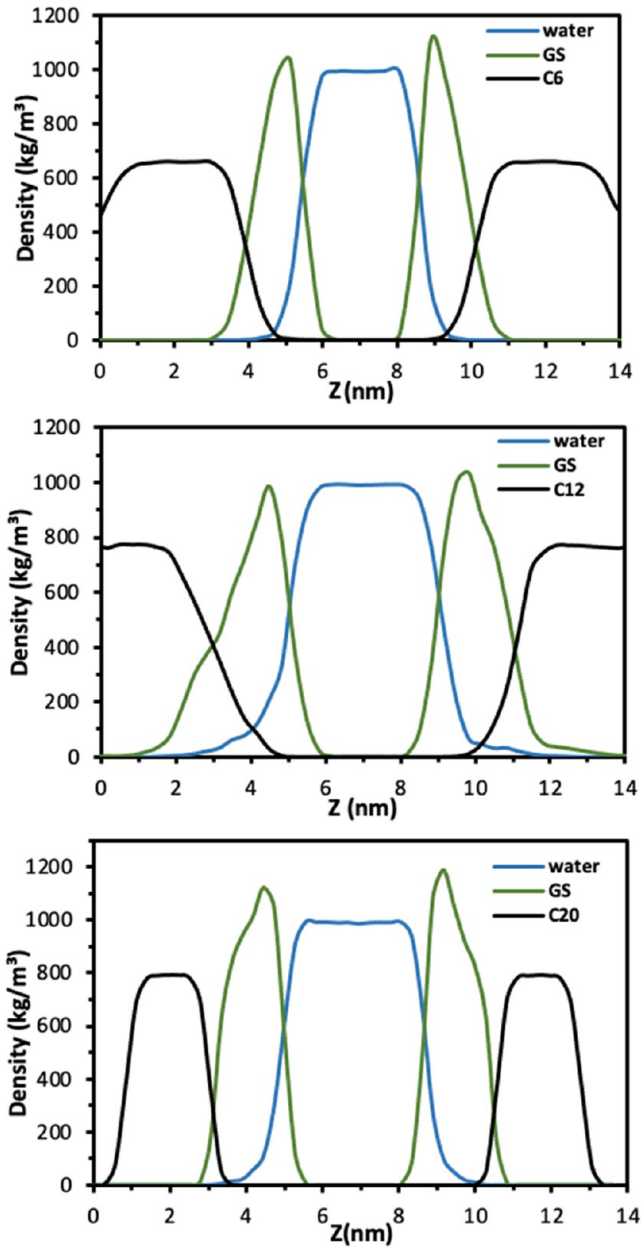

Figure 11. Density distribution of each component for C6-GS-Wt system (top), C12-GS-Wt system (middle), and C20-GS-Wt system (bottom).

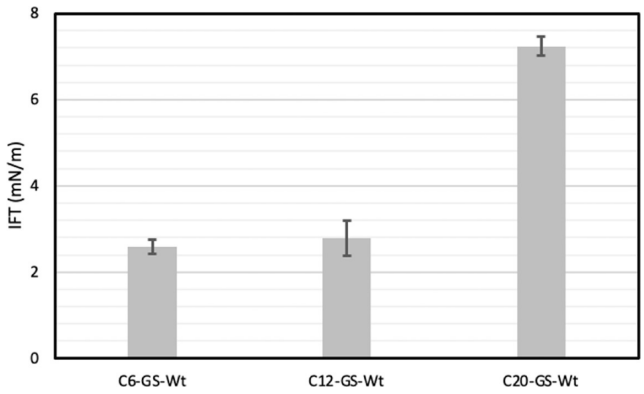

Figure 12. Change in the interfacial tension of each system.

$$E_{\mathrm{vdW}} = \sum_{ij}^{N} 4\varepsilon_{ij}\left[\left(\frac{\sigma_{ij}}{r_{ij}}\right)^{12} - \left(\frac{\sigma_{ij}}{r_{ij}}\right)^{6}\right] \tag{6}$$

$$E_{\mathrm{Coul}} = \sum_{ij}^{N} \frac{q_i q_j}{4\pi r_{ij}} \tag{7}$$

where E_{vdW} represents van der Waals interactions, E_{Coul} is the electrostatic interaction, ε_{ij} is the potential well depth, σ_{ij} is the distance at which there is minimal particle−particle interaction energy, r_{ij} is the distance between particles i and j, and q_i and q_j are the partial charges for particles i and j, respectively, and $i \neq j$.

The length of the straight chain within the oil molecules is the only factor used to distinguish among the three systems. Therefore, the interactions between GS and oil and water molecules will be discussed.

Figure 13a,b shows the changes in GS-GS (atom−atom) short-range interaction energy that accompany the GS micellization and the emulsification processes. The changes in the electrostatic interaction are much stronger than the vdW interaction, and therefore, electrostatic interactions play a dominant role in the micelle formation. During the initial 5 ns, the van der Waals attraction exhibited a substantial increase, transitioning from −2000 to −2500 kJ/mol for C6-GS-Wt, from −1500 to −3500 kJ/mol for C12-GS-Wt, and from −1500 to −4000 kJ/mol for C20-GS-Wt. This notable rise in attraction corresponds to the micelle dispersion process. Thereafter, in all systems except for C6-GS-Wt, the interaction between GS molecules remains stable for about 4 to 6 ns, with energy values of −3500 kJ/mol for C12-GS-Wt and −4000 kJ/mol for C20-GS-Wt. This suggests that GS interactions are not the primary driving force for the adsorption and migration of GS on the surface of the oil droplet (refer to Figure 13b). Following this, the energy values decreased to approximately −2800 kJ/mol for both C12-GS-Wt and C20-GS-Wt and remained at that value for all of the systems until the end of simulation. In particular, the differences seen in C20-GS-Wt, as shown in Figure 13b, can be attributed to the rearrangement of the hydrophobic chains of the GS molecules. However, in the C6-GS-Wt system, both the micellization and emulsification processes occurred more rapidly than in the other systems, Figure 2. Due to the higher dynamic motion of C6 molecules, GS molecules were compelled to interact with C6 molecules, leading to a slight separation among GS molecules; this effect can be clearly noticed from the Coulombic interaction values that are presented in Figures S3 and S5.

Figure 14a,b shows the changes in GS-oil (atom−atom) short-range interaction energy that accompany the GS micellization and the emulsification processes. Details of the interaction energy values for the last 50 ns in the three systems are provided in Table 3. The change in the electrostatic energy is significantly smaller than the calculated vdW energy between the GS micelles and oil molecules. This result confirms that vdW interactions are the primary driving force during the adsorption and emulsification processes, while electrostatic interactions do not play a significant role in these processes, as shown in Figure 14b. This fact is due to the oil molecules being able to easily engage in hydrophobic interactions with GS molecules and GS micelles. Moreover, the vdW energy in the emulsified systems becomes more negative because of the increased attractive forces between oil chains and GS chains. The results of Figures 13 and 14 suggest that emulsification occurs when there is not

https://doi.org/10.1021/acsomega.4c01332
ACS Omega 2024, 9, 27177−27191

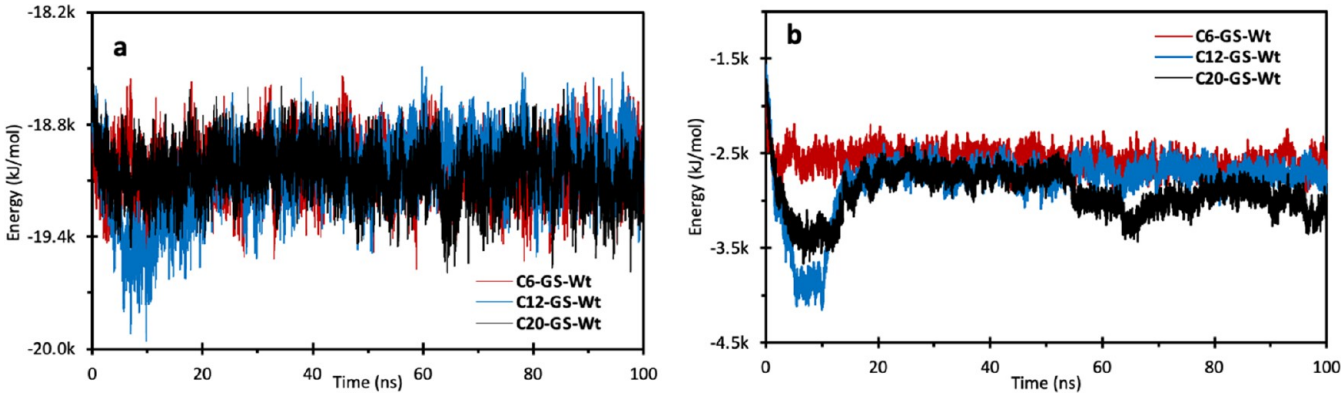

Figure 13. (a) GS-GS (Atom_Atom) electrostatic short-range interactions (Coul-SR). (b) GS-GS (Atom_Atom) van der Waals short-range interactions (LJ-SR).

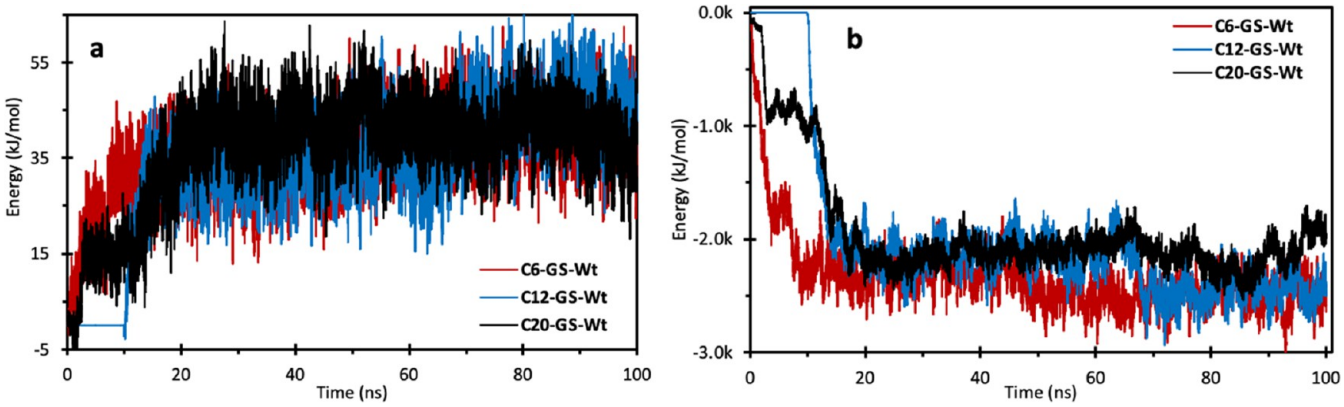

Figure 14. (a) GS-oil (Atom_Atom) electrostatic short-range interactions (Coul-SR). (b) GS-oil (Atom_Atom) van der Waals short-range interactions (LJ-SR).

Table 3. LJ Energy and Coulombic Energy Values between the GS Molecules and the Oil Molecules for the Three Systems

system	LJ energy (kJ/mol)	Coulombic energy (kJ/mol)
C6-GS-Wt	−2531.8 ± 159.1	37.0 ± 0.4
C12-GS-Wt	−2297.2 ± 266.2	39.7 ± 6.1
C20-GS-Wt	−2023.7 ± 69.0	38.1 ± 3.5

sufficient repulsion to keep the oil droplet and the GS micelles apart to distances where the van der Waals attraction decreased.

It can be concluded that emulsification depends on the magnitude of the attractive energy involved and does not matter if it is strong or weak. Figure 15a,b shows the changes in Oil−Oil (atom−atom) short-range interaction energy that accompany the emulsification of the oil droplet. In the C20-GS-Wt system, both electrostatic and vdW interactions are enhanced during the emulsification process. In this MD simulation, while preparing the oil droplet, C20 molecules do not exhibit a tendency to aggregate and create oil droplets. This behavior can be attributed to the reduction in hydrophobic interactions, also known as water-induced attraction between oil molecules,[63] which

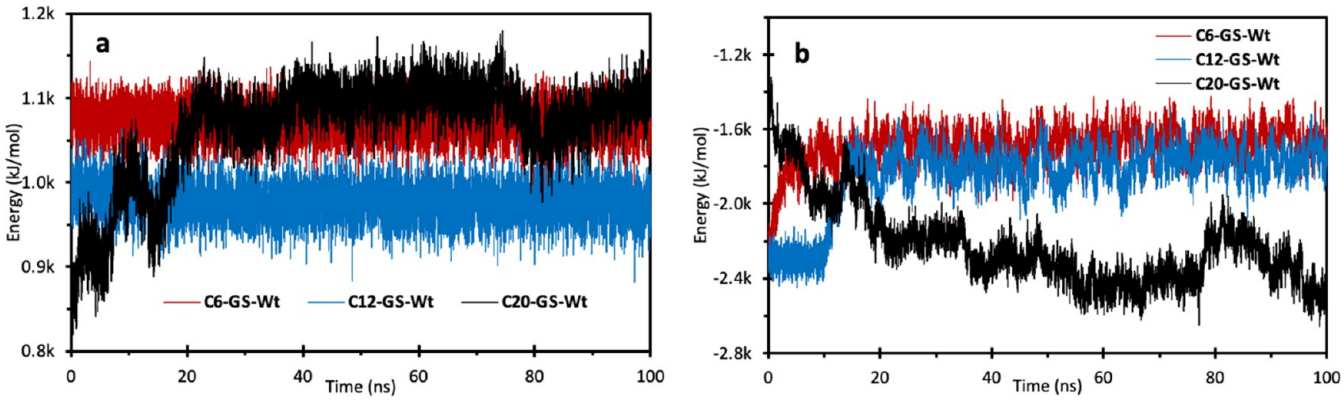

Figure 15. (a) Oil−oil (Atom_Atom) electrostatic short-range interactions (Coul-SR). (b) Oil−oil (Atom_Atom) van der Waals short-range interactions (LJ-SR).

https://doi.org/10.1021/acsomega.4c01332
ACS Omega 2024, 9, 27177−27191

diminish as the size of oil molecule increases (see Figure 15a). The hydrophobic segments of GS molecules become embedded within the interlayer structures of C6, C12, and C20 molecules, weakening their intermolecular interactions (Figure 15b). However, upon the introduction of GS molecules into the water/C20 molecules system, a notable change takes place. C20 molecules migrate toward the center of the oil droplet; close inspection of snapshots confirms this behavior, Figure 2.

The interactions between the oil−water molecules and the GS−water molecules were calculated. The energy values are an important parameter to judge the stability of the emulsified oil droplets, and the results are shown in Figures S6 and S7. So, 100 ns simulation times were enough to sample some localized properties such as the self-assembly process, micelle morphology, micelle adsorption, and emulsification of oil droplets.

CONCLUSIONS

Molecular dynamics (MD) simulations were employed to investigate the emulsification process of oil−water emulsions. This study focused on the introduction of green surfactant (GS) molecules to three diverse types of oils in a water environment. The study revealed a rapid aggregation of GS molecules into multiple clusters, each composed of several molecules. These clusters were subsequently adsorbed onto the surface of the oil droplets. Within this context, GS molecules were positioned at the oil−water interface, resulting in stable emulsified oil droplets within the aqueous medium. From the RMSD values of GS in the three systems, it can be concluded that GS molecules facilitate the spontaneous formation of stable micelles during the emulsification process. Since the GS hydrophilic segment contains hydroxyl groups, carboxylate groups, and amine groups, it makes the hydration layer of the oil droplet more stable and highly hydrophilic. RDF results predicted the number of hydration layers surrounding the emulsified oil droplets, which can improve the transfer of the emulsifying oil. The calculated diffusivities of the emulsifying different oil droplets were as follows: 0.001×10^{-5} cm^2/s for C6, 0.00095×10^{-5} cm^2/s for C12, and 0.00055×10^{-5} cm^2/s for C20 oil types. Changing the oil type affects interfacial tension, which suggests that interfacial tension is governed by hydrophobic interactions among the oil molecules. Our simulations suggest that electrostatic interactions play a dominant role in micelle formation and that vdW interactions play important roles in oil droplet emulsification. Introducing GS molecules to the C20-water system enhanced the aggregation tendency of C20 molecules for creating an oil droplet in a water medium, where C20 molecules migrate toward the center of the oil droplet. The emulsification performance of GS varies depending on the oil phase. GS showed optimal emulsification in the C6 oil phase with the highest diffusivity and lowest interfacial tension, indicating strong effectiveness in stabilizing emulsions with lighter oils. However, the performance was less efficient in the C12 and C20 oil phases, especially for C20, which had the lowest diffusivity and highest interfacial tension among the tested oil types.

These simulations provide valuable molecular-level insights into surfactant flooding relevant to green surfactants, enabling a deep analysis beyond traditional experiments. This study illustrates behaviors associated with microemulsion generation and interfacial adsorption processes in green surfactant systems, enhancing our understanding of oil displacement mechanisms, particularly with respect to green surfactants.

ASSOCIATED CONTENT

Supporting Information

The Supporting Information is available free of charge at https://pubs.acs.org/doi/10.1021/acsomega.4c01332.

Configuration diagrams at different simulation times (Figure S1); snapshots depicting the spontaneous aggregation of GS molecules (Figure S2); GS-GS (Atom_Atom) electrostatic short-range interactions (Coul-SR) for the three systems (Figure S3); count of hydrogen bonds between GS molecules and GS molecules with water molecules (Figure S4); GS-oil (Atom_Atom) electrostatic short-range interactions (Coul-SR) for the three systems (Figure S5); oil-Wt (Atom_Atom) electrostatic short-range interactions (Coul-SR), oil-Wt (Atom_Atom) van der Waals short-range interactions (LJ-SR) (Figure S6); GS-Wt (Atom_Atom) electrostatic short-range interactions (Coul-SR), GS-Wt (Atom_Atom) van der Waals short-range interactions (LJ-SR) (Figure S7); atomic partial charges for the GS molecule and the oil molecules (Figure S8) (PDF)

AUTHOR INFORMATION

Corresponding Author

Riyad Mahfud − *International college of engineering and management, Muscat 111, Oman;* orcid.org/0009-0007-2797-2861; Email: Riyad@icem.edu.om

Complete contact information is available at: https://pubs.acs.org/10.1021/acsomega.4c01332

Notes

The author declares no competing financial interest.

ACKNOWLEDGMENTS

This work was supported by the Research Council of Oman (MOHERI/BFP/ICEM/2023-24/04) and International College of Engineering and Management (IRG-ICEM2022/23-07). Special thanks go to Dr. Don Anton Balida for his valuable contributions and editing efforts.

REFERENCES

(1) Thomas, S. Enhanced Oil Recovery - An Overview. *Oil Gas Sci. Technol. - Rev. l'IFP* **2008**, *63*, 9−19.

(2) Gbadamosi, A. O.; Kiwalabye, J.; Junin, R.; Augustine, A. A review of gas enhanced oil recovery schemes used in the North Sea. *J. Pet. Explor. Prod. Technol.* **2018**, *8*, 1373−1387.

(3) Xu, X.; Saeedi, A.; Liu, K. An experimental study of combined foam/surfactant polymer (SP) flooding for carbone dioxide-enhanced oil recovery (CO2-EOR). *J. Pet. Sci. Eng.* **2017**, *149*, 603−611.

(4) Muggeridge, A.; Cockin, A.; Webb, K.; et al. Recovery rates, enhanced oil recovery and technological limits. *Philos. Trans. R. Soc., A* **2014**, *372*, No. 20120320, DOI: 10.1098/rsta.2012.0320.

(5) Massarweh, O.; Abushaikha, A. S. The use of surfactants in enhanced oil recovery: A review of recent advances. *Energy Rep.* **2020**, *6*, 3150−3178.

(6) Madani, M.; Zargar, G.; Takassi, M. A.; et al. Fundamental investigation of an environmentally-friendly surfactant agent for chemical enhanced oil recovery. *Fuel* **2019**, *238*, 186−197.

(7) Scott, M. J.; Jones, M. N. The biodegradation of surfactants in the environment. *Biochim. Biophys. Acta, Biomembr.* **2000**, *1508*, 235−251.

(8) Sarubbo, L. A.; Silva, M. d. G. C.; Durval, I. J. B.; et al. Biosurfactants: Production, properties, applications, trends, and general perspectives. *Biochem. Eng. J.* **2022**, *181*, No. 108377.

(9) Kurnia, I.; Zhang, G.; Han, X.; Yu, J. Zwitterionic-anionic surfactant mixture for chemical enhanced oil recovery without alkali. *Fuel* **2020**, *259*, No. 116236.
(10) Wu, Y.; Shuler, P.; Blanco, M.; Tang, Y.; Goddard, W. A. A Study of Branched Alcohol Propoxylate Sulfate Surfactants for Improved Oil Recovery. In *All Days*; SPE, 2005 DOI: 10.2118/95404-MS.
(11) Ren, Y.; Zhang, Q.; Yang, N.; et al. Molecular dynamics simulations of surfactant adsorption at oil/water interface under shear flow. *Particuology* **2019**, *44*, 36−43.
(12) Wei, Y.; Wang, X.; Dong, L.; et al. Molecular dynamics study on the effect of surfactant mixture on their packing states in mixed micelles. *Colloids Surf., A* **2021**, *631*, No. 127714.
(13) Hou, J.; Du, J.; Sui, H.; Sun, L. Surfactants Enhanced Heavy Oil−Solid Separation from Carbonate Asphalt Rocks-Experiment and Molecular Dynamic Simulation. *Nanomaterials* **2021**, *11*, 1835.
(14) Fu, L.; Gu, F.; Liao, K.; et al. Molecular dynamics simulation of enhancing surfactant flooding performance by using SiO2 nanoparticles. *J. Mol. Liq.* **2022**, *367*, No. 120404.
(15) Porzer, M.; Bujok, P.; Klempa, M.; Pánek, P. Evaluation of Surfactant Performance for Enhanced Oil Recovery *Geosci. Eng.* 2013; Vol. *59*.
(16) Wang, J.; Gu, F.; Han, W.; et al. Green Surfactant Made from Cashew Phenol for Enhanced Oil Recovery. *ACS Omega* **2023**, *8*, 2057−2064.
(17) Elraies, K. A.; Tan, I. M.; Awang, M.; Saaid, I. The Synthesis and Performance of Sodium Methyl Ester Sulfonate for Enhanced Oil Recovery. *Pet. Sci. Technol.* **2010**, *28*, 1799−1806.
(18) Imuetinyan, H.; Agi, A.; Gbadamosi, A.; Junin, R.; Oseh, J. Oil-water interfacial tension, wettability alteration and foaming studies of natural surfactant extracted from Vernonia Amygdalina. *Pet. Res.* **2022**, *7*, 350−356.
(19) Al-Ghamdi, A.; Haq, B.; Al-Shehri, D.; Muhammed, N. S.; Mahmoud, M. Surfactant formulation for Green Enhanced Oil Recovery. *Energy Rep.* **2022**, *8*, 7800−7813.
(20) Atilhan, M.; Aparicio, S. Molecular dynamics study on the use of Deep Eutectic Solvents for Enhanced Oil Recovery. *J. Pet. Sci. Eng.* **2022**, *209*, No. 109953.
(21) Wei, Y.; Wang, H.; Liu, G.; Wang, Z.; Yuan, S. A molecular dynamics study on two promising green surfactant micelles of choline dodecyl sulfate and laurate. *RSC Adv.* **2016**, *6*, 84090−84097.
(22) Suhendar, A.; Hertadi, R.; Alli, Y. MOLECULAR DYNAMICS STUDY OF OLEIC ACID-BASED SURFACTANTS FOR ENHANCED OIL RECOVERY. *Sci. Contrib. Oil Gas* **2018**, *41*, 125−135.
(23) Morán, M. C.; Pinazo, A.; Pérez, L.; et al. "Green" amino acid-based surfactants. *Green Chem.* **2004**, *6*, 233−240.
(24) Rostami, A.; Hashemi, A.; Takassi, M. A.; Zadehnazari, A. Experimental assessment of a lysine derivative surfactant for enhanced oil recovery in carbonate rocks: Mechanistic and core displacement analysis. *J. Mol. Liq.* **2017**, *232*, 310−318.
(25) Asl, H. F.; Zargar, G.; Manshad, A. K.; et al. Experimental investigation into l-Arg and l-Cys eco-friendly surfactants in enhanced oil recovery by considering IFT reduction and wettability alteration. *Pet. Sci.* **2020**, *17*, 105−117.
(26) Abraham, M. J.; Murtola, T.; Schulz, R.; et al. GROMACS: High performance molecular simulations through multi-level parallelism from laptops to supercomputers. *SoftwareX* **2015**, *1*−*2*, 19−25.
(27) Jorgensen, W. L.; Maxwell, D. S.; Tirado-Rives, J. Development and Testing of the OPLS All-Atom Force Field on Conformational Energetics and Properties of Organic Liquids. *J. Am. Chem. Soc.* **1996**, *118*, 11225−11236.
(28) Kaminski, G.; Duffy, E. M.; Matsui, T.; Jorgensen, W. L. Free Energies of Hydration and Pure Liquid Properties of Hydrocarbons from the OPLS All-Atom Model. *J. Phys. Chem. A* **1994**, *98*, 13077−13082.
(29) Briggs, J. M.; Nguyen, T. B.; Jorgensen, W. L. Monte Carlo simulations of liquid acetic acid and methyl acetate with the OPLS potential functions. *J. Phys. Chem. A* **1991**, *95*, 3315−3322.
(30) Sweere, A. J. M.; Fraaije, J. G. E. M. Accuracy Test of the OPLS-AA Force Field for Calculating Free Energies of Mixing and Comparison with PAC-MAC. *J. Chem. Theory Comput.* **2017**, *13*, 1911−1923.
(31) Mahfud, R.; Lacks, D.; Ishida, H.; Qutubuddin, S. Molecular Dynamic Simulations of Self-Assembly of Amphiphilic Comb-like Anionic Polybenzoxazines. *Langmuir* **2014**, *30*, 11858−11865.
(32) Zubillaga, R. A.; Labastida, A.; Cruz, B.; et al. Surface Tension of Organic Liquids Using the OPLS/AA Force Field. *J. Chem. Theory Comput.* **2013**, *9*, 1611−1615.
(33) Berendsen, H. J. C.; Grigera, J. R.; Straatsma, T. P. The missing term in effective pair potentials. *J. Phys. Chem. A* **1987**, *91*, 6269−6271.
(34) Braun, E.; Gilmer, J.; Mayes, H. B.; et al. Best Practices for Foundations in Molecular Simulations [Article v1.0]. *Living J. Comput. Mol. Sci.* **2019**, *1* (1), 5957 DOI: 10.33011/livecoms.1.1.5957.
(35) Berendsen, H. J. C.; Postma, J. P. M.; Van Gunsteren, W. F.; Dinola, A.; Haak, J. R. Molecular dynamics with coupling to an external bath. *J. Chem. Phys.* **1984**, *81*, 3684−3690.
(36) Parrinello, M.; Rahman, A. Crystal Structure and Pair Potentials: A Molecular-Dynamics Study. *Phys. Rev. Lett.* **1980**, *45*, 1196−1199.
(37) Kasturiarachi, A. B. Leap-frogging Newton's method. *Int. J. Math. Educ. Sci. Technol.* **2002**, *33*, 521−527.
(38) Cheatham, T. E. I. I. I.; Miller, J. L.; Fox, T.; Darden, T. A.; Kollman, P. A. Molecular Dynamics Simulations on Solvated Biomolecular Systems: The Particle Mesh Ewald Method Leads to Stable Trajectories of DNA, RNA, and Proteins. *J. Am. Chem. Soc.* **1995**, *117*, 4193−4194.
(39) Gao, Y.; Zhang, Y.; Yang, Y.; Zhang, J.; Gu, F. Molecular dynamics investigation of interfacial adhesion between oxidised bitumen and mineral surfaces. *Appl. Surf. Sci.* **2019**, *479*, 449−462.
(40) Deljooei, M.; Zargar, G.; Nooripoor, V.; Takassi, M. A.; Esfandiarian, A. Novel green surfactant made from L-aspartic acid as enhancer of oil production from sandstone reservoirs: Wettability, IFT, microfluidic, and core flooding assessments. *J. Mol. Liq.* **2021**, *323*, No. 115037.
(41) Martínez, L.; Andrade, R.; Birgin, E. G.; Martínez, J. M. PACKMOL: a package for building initial configurations for molecular dynamics simulations. *J. Comput. Chem.* **2009**, *30*, 2157−2164.
(42) Fujiwara, S.; Itoh, T.; Hashimoto, M.; Horiuchi, R. Molecular dynamics simulation of amphiphilic molecules in solution: micelle formation and dynamic coexistence. *J. Chem. Phys.* **2009**, *130*, No. 144901.
(43) Mallamace, F.; Gambadauro, P.; Micali, N.; et al. Kinetic Glass Transition in a Micellar System with Short-Range Attractive Interaction. *Phys. Rev. Lett.* **2000**, *84*, 5431−5434.
(44) Yuan, J.; Zhong, L.; Vakili, M.; Segun, G. A. New modeling method to simulate asphaltenes at oil sands process in water management. *J. Mol. Graph. Model.* **2019**, *91*, 1−9.
(45) Shrake, A.; Rupley, J. A. Environment and exposure to solvent of protein atoms. Lysozyme and insulin. *J. Mol. Biol.* **1973**, *79*, 351−371.
(46) Ma, J.; Yang, Y.; Li, X.; Sui, H.; He, L. Mechanisms on the stability and instability of water-in-oil emulsion stabilized by interfacially active asphaltenes: Role of hydrogen bonding reconstructing. *Fuel* **2021**, *297*, No. 120763.
(47) Huang, B.; Nan, X.; Fu, C.; et al. Probing the Coalescence Mechanism of Oil Droplets in Fluids Produced by Oil Wells and the Microscopic Interaction between Molecules in Oil Films. *Energies* **2022**, *15* (12), 4274 DOI: 10.3390/en15124274.
(48) Smith, A.; Dong, X.; Raghavan, V. An Overview of Molecular Dynamics Simulation for Food Products and Processes. *Processes* **2022**, *10* (1), 119 DOI: 10.3390/pr10010119.
(49) Müller, P.; Bonthuis, D. J.; Miller, R.; Schneck, E. Ionic Surfactants at Air/Water and Oil/Water Interfaces: A Comparison Based on Molecular Dynamics Simulations. *J. Phys. Chem. B* **2021**, *125*, 406−415.
(50) Belhaj, A. F.; Elraies, K. A.; Mahmood, S. M.; et al. The effect of surfactant concentration, salinity, temperature, and pH on surfactant adsorption for chemical enhanced oil recovery: a review. *J. Pet. Explor. Prod. Technol.* **2020**, *10*, 125−137.
(51) Takeda, K.; Andoh, Y.; Shinoda, W.; Okazaki, S. Molecular Behavior of Linear Alkylbenzene Sulfonate in Hydrated Crystal, Tilted

Gel, and Liquid Crystal Phases Studied by Molecular Dynamics Simulation. *Langmuir* **2019**, *35*, 10877−10884.
(52) Hunter, M. A.; Demir, B.; Petersen, C. F.; Searles, D. J. New Framework for Computing a General Local Self-Diffusion Coefficient Using Statistical Mechanics. *J. Chem. Theory Comput.* **2022**, *18*, 3357−3363.
(53) Santos, M. S.; Hamza, M.; Mercier Franco, L. F.; Castier, M.; Economou, I. Molecular Understanding of Enhanced Hydrocarbon Recovery Processes: Role of Local Self-Diffusion Coefficients of Complex Mixtures. *Energy Fuels* **2022**, *36* (15), 8301−8310, DOI: 10.1021/acs.energyfuels.2c01031.
(54) Onaizi, S. A.; Alsulaimani, M.; Al-Sakkaf, M. K.; et al. Crude oil/water nanoemulsions stabilized by biosurfactant: Stability and pH-Switchability. *J. Pet. Sci. Eng.* **2021**, *198*, No. 108173.
(55) Nicoli, D. F.; De Buzzaccarini, F.; Romsted, L. S.; Bunton, C. A. Measurement of the correlation radius in oil-in-water microemulsions by dynamic light scattering. *Chem. Phys. Lett.* **1981**, *80*, 422−426.
(56) Saien, J.; Moghaddamnia, F.; Bamdadi, H. Interfacial Tension of Methylbenzene−Water in the Presence of Hydrophilic and Hydrophobic Alumina Nanoparticles at Different Temperatures. *J. Chem. Eng. Data* **2013**, *58*, 436−440.
(57) Li, X.; Ross, D. A.; Trusler, J. P. M.; Maitland, G. C.; Boek, E. S. Molecular dynamics simulations of CO2 and brine interfacial tension at high temperatures and pressures. *J. Phys. Chem. B* **2013**, *117*, 5647−5652.
(58) van Buuren, A. R.; Marrink, S. J.; Berendsen, H. J. C. A molecular dynamics study of the decane/water interface. *J. Phys. Chem. A* **1993**, *97*, 9206−9212.
(59) Jacobs, M.; Liang, H.; Pugnet, B.; Dobrynin, A. V. Molecular Dynamics Simulations of Surface and Interfacial Tension of Graft Polymer Melts. *Langmuir* **2018**, *34*, 12974−12981.
(60) Shi, P.; Luo, H.; Tan, X.; et al. Molecular dynamics simulation study of adsorption of anionic−nonionic surfactants at oil/water interfaces. *RSC Adv.* **2022**, *12*, 27330−27343.
(61) Haynes, W. M. *Edition 95*. *Journal of the American Pharmaceutical Association* (1942).
(62) Bergfreund, J.; Bertsch, P.; Fischer, P. Effect of the hydrophobic phase on interfacial phenomena of surfactants, proteins, and particles at fluid interfaces. *Curr. Opin. Colloid Interface Sci.* **2021**, *56*, No. 101509, DOI: 10.1016/j.cocis.2021.101509.
(63) Chandler, D. Hydrophobicity: Two faces of water. *Nature* **2002**, *417*, 491.

https://doi.org/10.1021/acsomega.4c01332
ACS Omega 2024, 9, 27177−27191